www.sciencemag.org/cgi/content/full/1178105/DC1

Supporting Online Material for

Detection of Adsorbed Water and Hydroxyl on the Moon

Roger N. Clark

E-mail: rclark@usgs.gov

Published 24 September 2009 on *Science* Express
DOI: 10.1126/science.1178105

This PDF file includes:

Materials and Methods
SOM Text
Figs. S1 to S6
References

Detection of Adsorbed Water and Hydroxyl on the Moon

Roger N. Clark
U. S. Geological Survey, MS 964, Box 25046 Federal Center, Denver CO 80227

1178105 Supplementary Online Material

Contents

The VIMS Data
Thermal Modeling and Thermal Removal
Laboratory Analyses of Water Content
Viewing Geometry Effects
Acknowledgement
Figures
References

The VIMS Data

Cassini VIMS is described by (1). The following VIMS image cubes were used:

1) 1313633519.230-131041,
2) 1313633580.230-131130,
3) 1313633642.230-131220,
4) 1313633704.230-131311,
5) 1313633766.230-131401,
6) 1313633828.230-131450,
7) 1313633891.230-131540,
8) 1313633953.230-131630,
9) 1313634015.230-131720,
10) 1313634077.230-131809,
11) 1313634139.230-131859.

The above cubes are each 64x64 pixels. The moon drifted through the field of view during the fly-by. The time period covered was 1999-230T02:05:11.747 to 1999-230T02:16:34.098 (year, day of year, T, spacecraft event time). These 11 cubes were the only cubes where the entire moon was within the VIMS field of view. Exposure times were the shortest possible; 13 milliseconds/pixel for the infrared channel (IR). The visible channel was commanded to follow the scan time of the IR, resulting in an exposure time of 320 milliseconds/line. Each cube was divided by the VIMS pipeline 2009 flat field and multiplied by the latest VIMS calibration multiplier (called RC17).

Because VIMS was designed to operate at Saturn, the bright moon saturated the sensor at many wavelengths. Operating this close to the sun, VIMS was also operating at a higher temperature than it does at Saturn. IR detector temperatures were 80 and 81K, while the optics temperature sensors were 196 and 180 K. These higher optics temperatures resulted in sensor saturation for wavelengths beyond 3.8 μm from thermal emission generated in the instrument. High signals from lunar thermal emission and high thermal

background led to sensor saturation and non-linearity beyond about 3.4 μm. The ~1 to ~1.6-μm region was completely saturated (Fig. S1).

The 11 VIMS image cubes were re-sampled by nearest neighbor then hand registered to approximately 1/10th pixel. The 11 cubes were combined by averaging. This resulted in a higher signal-to-noise ratio data set with higher apparent spatial resolution. Several individual image cubes were also analyzed and gave similar, but lower signal-to-noise ratio results.

Thermal Modeling and Thermal Removal

The thermal removal followed the method in (2) and includes extrapolating the lunar spectrum to longer wavelengths (Fig. S2). The thermal model (2) was verified for this study with a laboratory experiment by measuring the radiance from a heated basalt and comparing the model prediction to the observed reflected + thermal emission (Fig. S3). This test included greater thermal contribution (by ~8x) than observed in the VIMS lunar data. Derived lunar temperatures in the VIMS data ranged from ~270 to as much as 375K (Fig. 1D). Temperatures near 375 K can increase observed intensities at 3-μm by 25%. However, at higher latitudes and lower sun angles, temperatures drop below about 300 K and thermal emission becomes minor at 3-μm and at shorter wavelengths in the presence of sunlight (Fig. 2A, spectrum sp3).

The added thermal component has a predictable effect on the lunar spectra and can not create apparent water or hydroxyl absorptions over the spectral range covered by VIMS. Thermal emission works to diminish observed absorptions due to features in the spectral emissivity. Absorption features in reflectance, R, appear as emission features in emissivity, e, from Kirchoff's law, $e = 1 - R$. Spectral features added to the thermal spectrum due to the emissivity of the lunar surface are corrected by the thermal model which includes derivation of emissivity. The thermal removal algorithm first estimates the thermal emission as an excess of apparent reflectance beyond 3.2 μm (Fig. S2) and removes the excess to continue the trend in observed reflectance from shorter wavelengths by extrapolation of the apparent continuum. The algorithm is constrained so that it will not remove a greater amount of thermal emission artificially creating a downturn beyond 3-μm. The probable error in the derived reflectance decreases toward shorter wavelengths because the thermal component is weaker at those wavelengths (Figure 2A). After the first thermal removal, the derived reflectance spectrum, R, is used to make a new spectral emissivity estimate, e, from Kirchoff's law, $e = 1 - R$ (Fig. S2). The emissivity spectrum and this first iteration derived reflectance spectrum is then used to compute the second estimate of the temperature. The new thermal emission spectrum is computed and the thermal emission is removed. The second correction will compensate for infilling of any absorption features by thermal emission and spectral features in the emissivity spectrum. In the lunar case, because the thermal contribution is small at 3 microns, the infilling is also small, at least for all spectra investigated in the VIMS data set.

Laboratory Analyses of Water Content

The main paper discusses absorption strengths of water with different radiative transfer models. Another study was conducted using a laboratory sample of basalt. The basalt was dehydrated, driving off adsorbed water, measuring spectra before and after heating. The weight difference from before and after indicated the amount of water lost during heating in a vacuum. Fig. S4 shows the results and the results are discussed in the main paper.

Viewing Geometry Effects

The VIMS data indicates higher water/OH band depths near the lunar terminator. While this might be evidence for water moving with the diurnal cycle on the moon, simpler explanation may be effects from varying viewing geometry. Enhanced absorption bands have been observed in imaging spectroscopy maps of other objects. For example, the band depth for the 1.04-μm ice absorption for the Saturnian satellite Enceladus appears stronger near the terminator (Fig. S5). At the temperatures of Enceladus, < 90 K, and short diurnal cycle, 1.37 days, water can not be moving in the abundance or grain size required to explain the increased absorption strength. Because the abundance of ice on Enceladus is high, >90% (3), the ice grain size would need to change to explain changes in feature strength. To explain such changes in band depth, the ice grains would need to be changing, both increasing and decreasing in size by an order of magnitude over the diurnal cycle, which is not possible at the low temperatures.

An alternative explanation to changing water abundance or ice grain size is viewing geometry effects. At low solar incidence angles, high topography will be illuminated and low topography will be in shadow, but illuminated by the sunlit high topography. A 6.3-centimeter diameter crater was constructed in the lab using the same basalt as used in Fig. S3 and spectra were obtained on the lit and shadowed side of the crater at varying incidence angles. The observed band depths at high incidence angles illustrate the effects of multiple reflections from the crater walls. Both lit and unlit sides of the crater show enhanced band strengths at high incidence angles, simulating effect near the terminator on the Moon.

Acknowledgement

I thank Neal Pearson for assistance in measuring the basalt experiments in Figures S3 and S6. This research was funded by NASA Cassini VIMS under contract to the U. S. Geological Survey, R. Clark, VIMS Team Member.

Figures

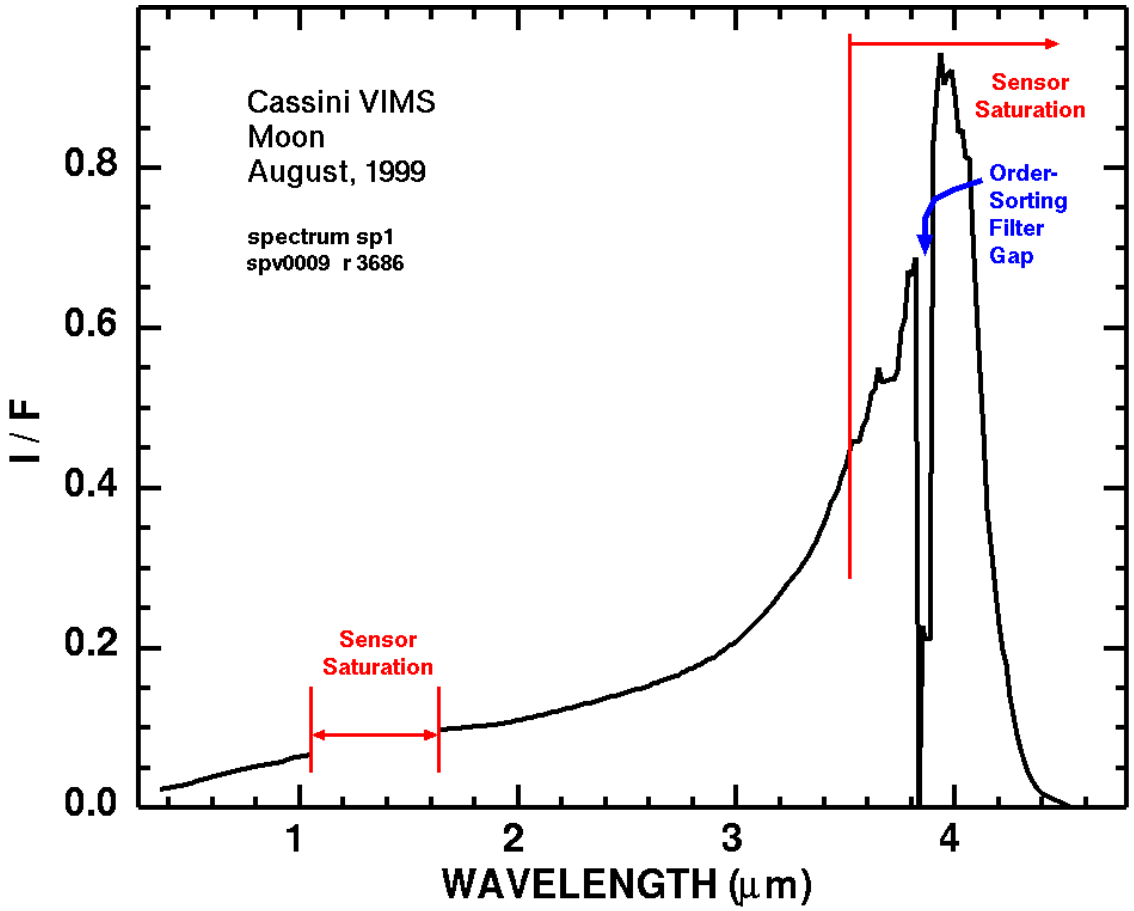

Fig. S1. An example VIMS spectrum (spectrum sp1 from Fig. 1) showing that the overall calibration of the VIMS and saturated signal regions.

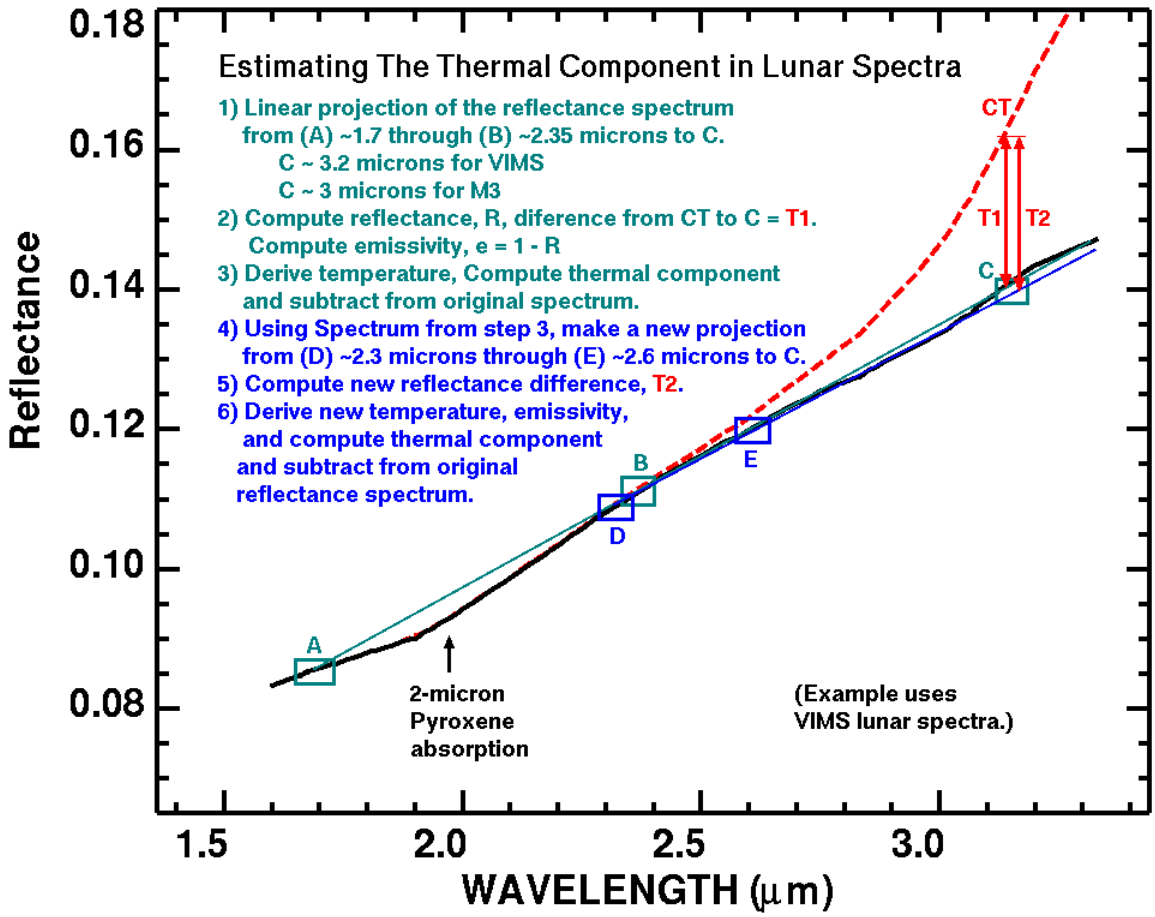

Fig S2. Illustration of the thermal removal procedures.

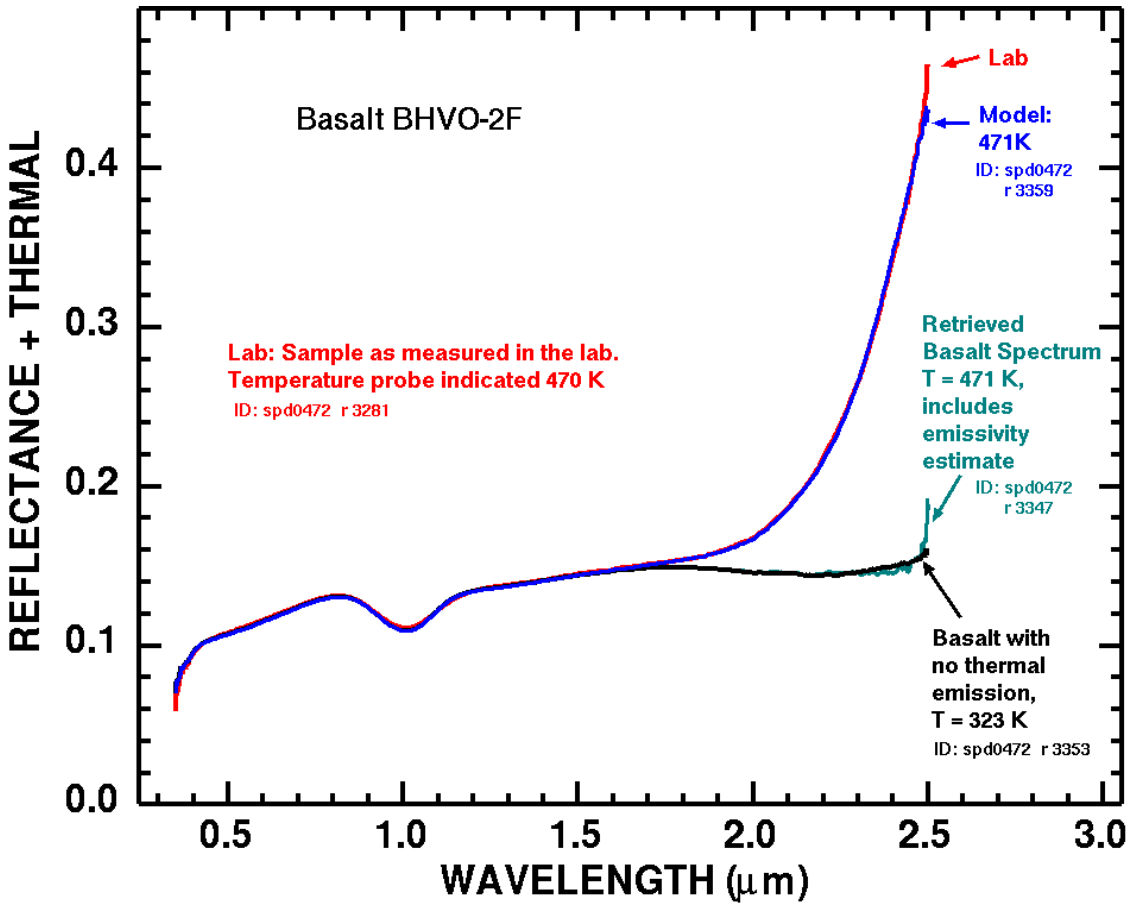

Fig. S3. Test of the methods for removing thermal emission. Spectra of a basalt heated and at room temperature. The model follows the methodology in (2) and illustrates that the thermally removed spectrum (green line) closely matches the spectrum measured at lower temperatures (black line).

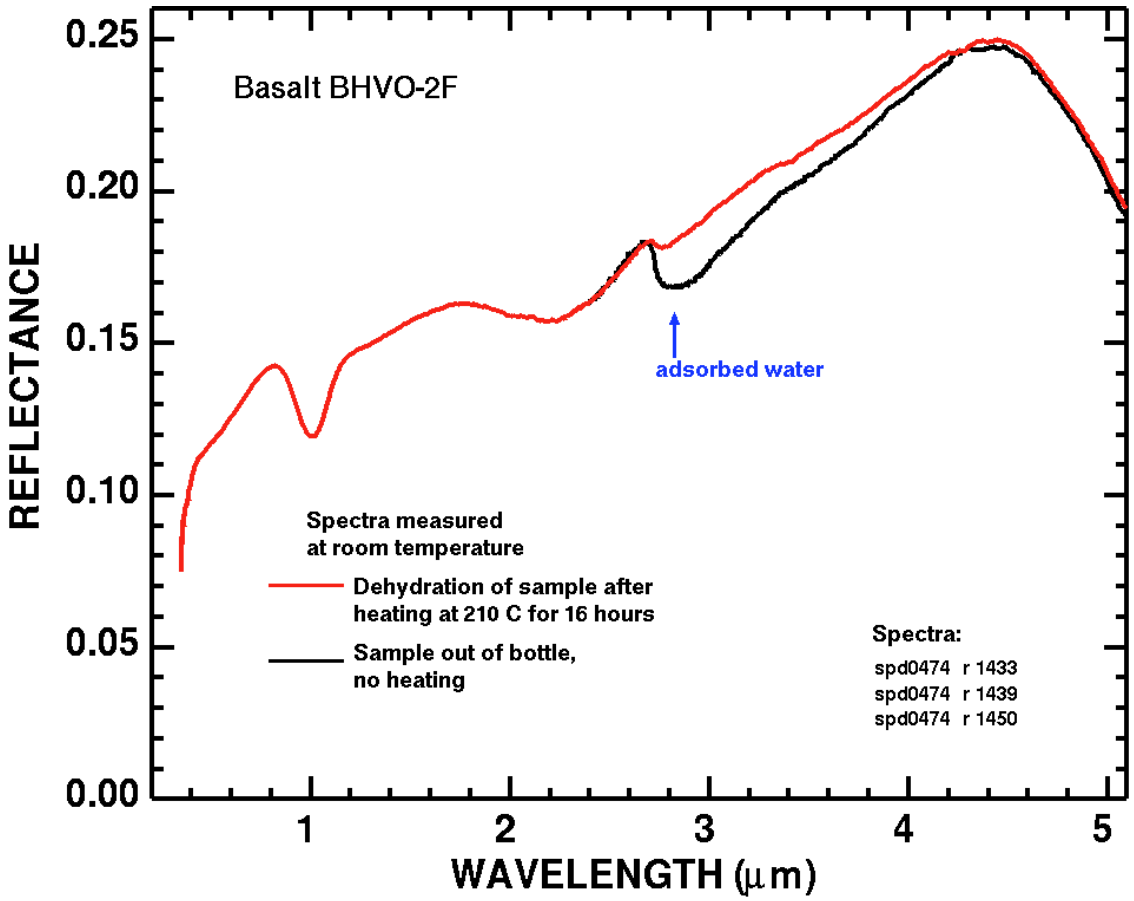

Figure S4. Laboratory spectra of a Hawaiian basalt showing dehydration of adsorbed water upon heating in a vacuum. The broad absorption bands near 1 and 2 μm are due to the mineral pyroxene while the absorption near 3 μm is due to water. The position where the water begins absorbing at 2.7 μm closely matches the position where water begins absorbing in the VIMS lunar spectra although the hydrogen bonding in this sample is lower than that observed in VIMS data so the shape and position are slightly different. Approximately 2,500 ppm water was removed in the dehydration sequence. The sample was dehydrated in a vacuum between 480 and 500 K for 16 hours.

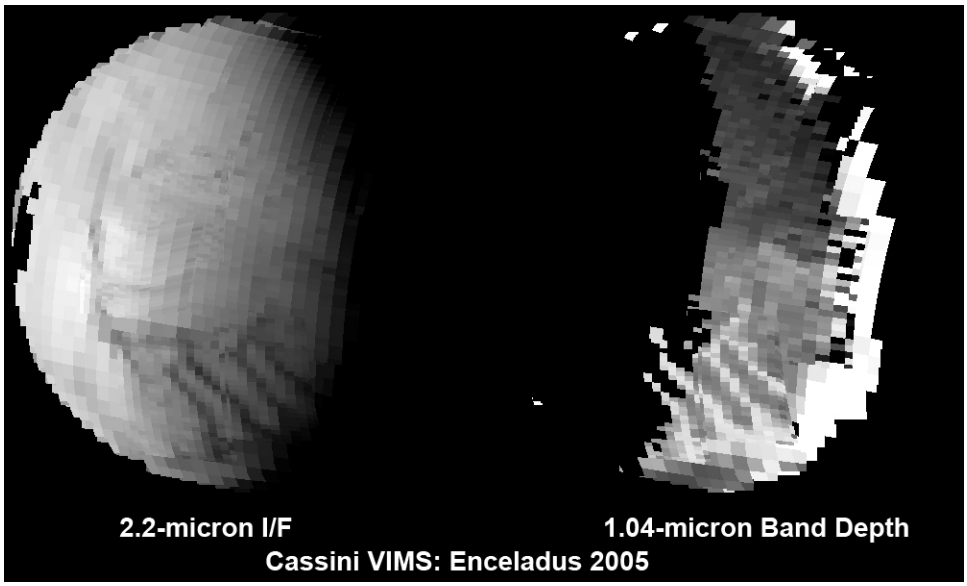

Fig. S5. The 1.04-μm band depth (right) of the Saturnian moon Enceladus observed by Cassini VIMS. Observation described by (3). A 2.2-μm I/F image is shown on the right for comparison. VIMS shows increased band depth near the terminator, illustrating viewing geometry effects. The left half of the band depth image was saturated at 1-μm.

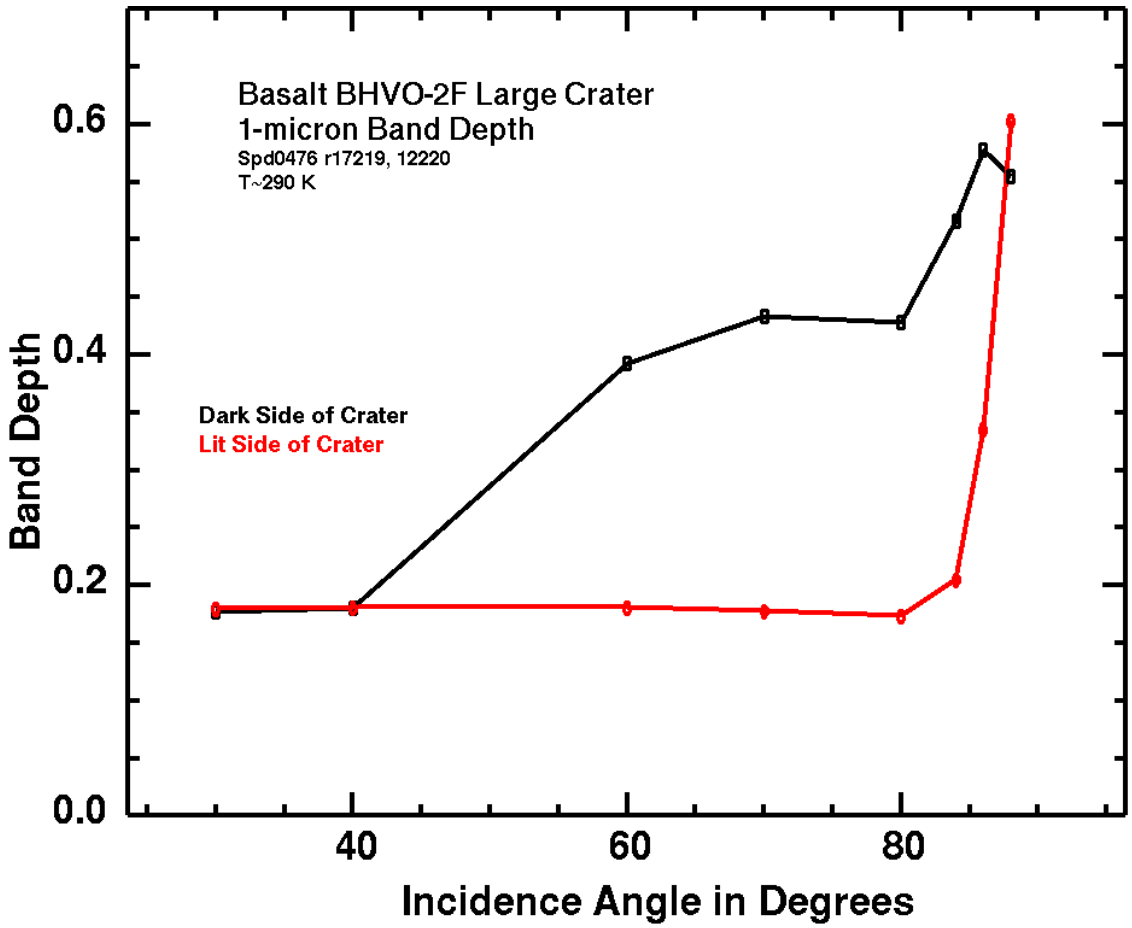

Fig. S6. Viewing geometry affects apparent band depth. At low sun angles, multiple reflections of sunlit topography into shadowed areas cause reflectance squared and higher order effects, increasing band depth.

References

1) R.H., Brown, K.H. Baines, G. Bellucci, J.P. Bibring, B.J. Buratti, F. Capaccioni, P., Cerroni, P., Clark, R.N., A. Coradini, D.P. Cruikshank, P. Drossart, V. Formisano, R. Jaumann, Y. Langevin, D.J. Matson, T.B. McCord, V. Manella, E. Miller, R.M. Nelson, P.D. Nicholson, B. Sicardy, and C. Sotin, *Space Science Reviews*, **115**, 111-168, (2004).

2) Clark, R. N., *Icarus*, **40**, 94-103, (1979).

3) R. H.,Brown, R. N. Clark, B. J. Buratti, D. P. Cruikshank, J. W. Barnes, R. M. E. Mastrapa, J. Bauer, S. Newman, T. Momary, K. H. Baines, G. Bellucci, F. Capaccioni, P. Cerroni, M. Combes, A. Coradini, P. Drossart, V. Formisano, R. Jaumann, Y. Langevin, D. L. Matson, T. B. McCord, R. M. Nelson, P. D. Nicholson, B. Sicardy, C. Sotin, *Science*, **311**, 1425-1428, (2006).